Construction and Building Materials 409 (2023) 133868

Contents lists available at ScienceDirect

Construction and Building Materials

journal homepage: www.elsevier.com/locate/conbuildmat

On the role of alkali content on one-part alkali activated slag pastes produced with tri- blend solid activators

D. Coffetti [a,*], S. Candamano [b], F. Crea [b], L. Coppola [a]

[a] Department of Engineering and Applied Sciences, University of Bergamo, Italy
[b] Department of Mechanical, Energy and Management Engineering – DIMEG, University of Calabria, Italy

ARTICLE INFO

Keywords:
Alternative binders
Alkali-activated materials
Blast furnace slag
Slag cements
Sodium carbonate

ABSTRACT

The paper investigates the effect of tri-blend solid alkaline activators, based on sodium metasilicate pentahydrate, potassium hydroxide and sodium carbonate, on the physico-chemical features, the fresh and hardened performances of activated slag pastes prepared with the one-part methodology. Specifically, the alkali to slag ratio (Ac) and the total amount of the selected activators were varied at a fixed water/binder ratio, molar silica modulus (Ms) and relative mass activators ratio. Microstructures and reaction products were analyzed by means of X-ray diffraction, thermogravimetry, scanning electron microscopy and FT-IR. Fresh and elasto-mechanical properties of pastes were also evaluated. Amorphous calcium carbonate (ACC) as well as metastable vaterite were found in low reacted systems, produced by the preferential early-age reaction between dissolved carbonate ions present in the pore solution and the calcium ions released by the partial dissolution of the slag and stabilized by a sufficient high concentration of magnesium in the pore solution, not consumed to the form hydrotalcite. Sodium carbonate failed in extending the pot life of the investigated systems. The optimal alkali content was found to be close to 0.075 as it determines the development of compact and dense microstructure (2025 kg/m^3), the maximum elasto-mechanical properties (elastic modulus of 26.1 GPa and compressive strength of 102.8 MPa at 28 days) and it allows to produce flowable mixtures (200 mm).

1. Introduction

Since the '90 s, several new binders have been proposed as environmentally friendly materials and have been investigated to manufacture Portland-free mortars and concretes [1], such as super-sulphated cements [2], calcium sulphoaluminate cements [3–5], alkali activated materials [6,7] including geopolymers [8–10]. Among these, ground granulated blast furnace slag (GGBFS), an industrial by-products from steel industry, in combination with alkaline activators, has been successfully used to produce sustainable binders [11]. Conventional alkali-activated slag (AAS) systems are obtained by a reaction of an aqueous solution of alkali hydroxides and silicates with the solid calcium-rich aluminosilicate precursor. Nevertheless, the alkali activator solutions are corrosive, viscous and hazardous, all factors that make them practically useless in the in-situ application. For this reason, the development of one-part alkali-activated binders, where only a dry blend of precursors and activators in powder form is used in addition to water, is needed to improve the safety of workers and to enhance the commercial viability and large-scale applications of the alkali activated materials in the construction industry [6,12].

Actually, several papers discuss various aspect and applications of two-part AAS systems [13–19], but only a limited number of articles deals with the properties of one-part alkali activated slag binders [20–24]. Ravikumar et al. [25] investigated the properties of one-part AAS mortars cured at ambient temperature with Na_2O to slag ratios (n) equal to 0.05–0.15–0.25 and SiO_2 to Na_2O ratios (Ms) of 0.6 and 1.5, obtained by mixing anhydrous sodium silicate ($Ms = 1.95$) and NaOH powders. They compared the measured properties to those achieved by mortars manufactured with the same mix design but preliminarily dissolving powders in water at ambient temperature. Authors demonstrated that compressive strengths decrease, in both the tested procedures, greater than those that can be achieved by using commercial waterglass solutions. They attributed the reduction in compressive strength to the incomplete dissolution of sodium silicate, thus demonstrating, as general indication, that rules for a proper design of AAS binders are not immediately applicable to one-pot systems.

It is also widely accepted that amount and type of activators not only affect the AAS binder properties, but they also represent the main source

* Corresponding author
E-mail address: denny.coffetti@unibg.it (D. Coffetti).

https://doi.org/10.1016/j.conbuildmat.2023.133868
Received 16 August 2023; Received in revised form 30 September 2023; Accepted 17 October 2023
Available online 21 October 2023

of their environmental footprint. Among activators, sodium carbonate is an eco-friendly alternative that can rise pH to values suitable to activate slag. It is 2–3 times cheaper than NaOH or sodium silicate and it can be obtained either as a secondary product from industrial processes or refined from natural raw materials, such as trona, by moderate temperature thermal treatment [26]. However, Na_2CO_3-activated slag binders are characterized by high setting times and slow development of mechanical properties than NaOH or sodium silicate-activated ones [27]. The behavior can be attributed to the initial reaction between CO_3^{2-} from the activator and Ca^{++} leached from slag to form calcium and sodium/calcium carbonate double salts [28], followed by increasing of alkalinity due to release of hydroxide ions. Bernal et al. [27] demonstrated that setting and hardening of alkali-carbonate activated slags can be achieved within the first 24 h after an overall induction period of 12 h through the addition of sodium silicate. However, the above-mentioned experimental campaign was carried out using sodium metasilicate and sodium carbonate solutions that were mixed separately with the anhydrous slag in a content of 8 g activators (50 wt% sodium carbonate/50 wt% sodium metasilicate) per 100 g of slag. Furthermore, carbonates including pirssonite, vaterite, aragonite and calcite were identified along with the zeolites hydroxysodalite and analcime at early times of reaction.

Starting from the aforementioned findings, in this study authors propose a different blend of solid activators, based on sodium metasilicate pentahydrate, potassium hydroxide and sodium carbonate, with the aim to furtherly widen the database of knowledge of one-part AAS binder. Sodium metasilicate ($Ms = 1$) benefits of a high dissolution rate and thus is readily soluble in water, whereas amorphous silicate glasses ($Ms = 2$–3), are only slightly attacked by water at ambient temperatures. The fast dissolution of the sodium silicate powder supplies silicate species to the reacting system thus consuming Ca^{++} leached from slag to form hydration products. The process promotes a further Ca^{++} dissolution. It is beneficial to the development of mechanical properties within certain extent, but excessive reaction rates can shorten pot life as well. Potassium hydroxide is used in partial replacement of sodium hydroxide to reduce efflorescence in pastes and mortars, because potassium is more strongly bound to the gel frameworks [29] and also because potassium carbonate crystals are usually less visually evident than their sodium counterparts [30]. Moreover, the partial replacement of K(OH) with Na_2CO_3 has been carried out to decrease the environmental footprint of the activators and investigate its effect on setting time of the mixtures.

Currently, the understanding of using blended activators remains quite limited, with only a sparse number of articles providing insights in this area [31–34]. Nevertheless, to promote the adoption of one-part alkali-activated binders as a substitute for Portland cement, it becomes imperative to utilize blended activating materials. This approach allows for the customization of the properties of AAS mortars and concretes to meet specific requirements.

For this reason, the development of the physico-chemical features, the fresh and hardened performances of slag pastes prepared with the one-part methodology have been investigated by varying the alkali to slag ratio (Ac) and the total amount of the selected activators at a fixed water/binder ratio and molar silica modulus (Ms).

2. Materials and methods

2.1. Materials

Ground granulated blast furnace slag with a 28-day pozzolanic activity index equal to 0.76 (according to EN 15167-1 and EN 196-5) was used as precursor.

Physical properties and chemical/mineralogical composition of slag cement were investigated by means of laser granulometry (Mastersizer 3000 Malven Instruments Ltd), XRD analysis (Rigaku Miniflex 60, X-ray source Cu K-α (0.15418 nm), 40 kV 15 mA, θ step 0.02, rate 1°/min) and SEM-EDS measurements (Inspect, FEI company). The GGBFS particles have a specific mass equal to 3.13 g/cm^3, an average size of 12.42 μm (Fig. 1) and a specific surface equal to 345 m^2/kg.

Moreover, the XRD pattern shows a typical amorphous hump around 25° and 35° 2θ (Fig. 1) that reflects the short range order of CaO-Al_2O_3-MgO-SiO_2 glass structure as reported by Wang and Scrivener [35]. The slag is characterized by dense, sharp-edged grains (Fig. 1).

Chemical composition of the slag, in terms of oxides and obtained by Energy-dispersive X-ray spectroscopy (EDS) is reported in Table 1.

Furthermore, starting from the chemical composition of GGBFS (Table 1), the basicity coefficient Kb (Eq. (1)) and the quality coefficient Kq (Eq. (2)) were calculated according to [36]:

$$Kb = \frac{CaO + MgO}{SiO_2 + Al_2O_3} = 1.20 \quad (1)$$

$$Kq = \frac{CaO + MgO + Al_2O_3}{SiO_2 + TiO_2} = 1.77 \quad (2)$$

Sodium metasilicate pentahydrate (Silmaco), potassium hydroxide (Produits Chimiques de Loos) and sodium carbonate (Solvay) were all of industrial grade (total impurities < 1 %). Tap water at 20 °C was used to produce pastes.

2.2. Mixture proportioning and mixing

The alkaline tri-blend activator, already used by the authors to produce a lightweight AAS plaster for the retrofitting of existing buildings [37], was obtained by mixing sodium metasilicate pentahydrate, potassium hydroxide and sodium carbonate powders in a relative mass ratio equal to 7: 3: 1. Seven different AAS mixtures (Table 2) were prepared by varying the alkali content (Ac, Eq. (3)) between 0 % and 15 % (equal to a/p: activator/precursor ratio between 0 and 22 %) in order to investigate the rheological, microstructural and elasto-mechanical properties of slag cement-based mixtures. The maximum activator/precursor ratio was limited to ensure both environmental and economic sustainability.

$$Ac = \frac{Na_2O + K_2O}{GGBFS} wt.\% \quad (3)$$

The molar silica modulus (Ms, Eq. (4)) of the powdered activators were kept constant at 0.48 and sodium carbonate was used to partially replace sodium silicate and Na_2O powders [38]. Water/total solids ratio (w/s) of pastes was fixed at around 0.30.

$$Ms = \frac{SiO_2}{Na_2O + K_2O} \quad (4)$$

Alkali activated pastes were prepared using a mixer with planetary motion in accordance with "Dry mixing method" proposed by Bayuaji *et al.* [39]. In particular, the mixing procedure followed five steps: i) the slag cement, alkali activators in powder or flakes and water are placed into the bowl; ii) the mixer starts mixing at low speed for 30 s; iii) the mixing proceeds at high speed for 60 s; iv) the mixing stops for 90 s; v) the mixing procedure is completed for further 60 s at high speed.

2.3. Fresh state tests

Workability was measured on pastes by means of flow table according to EN 1015–3. In addition, specific mass on fresh mixtures according to EN 1015–6 standard was evaluated. Furthermore, the pot life of mixtures, that corresponds the time during which the workability by flow table is higher than 60 % respect to initial consistency, was measured.

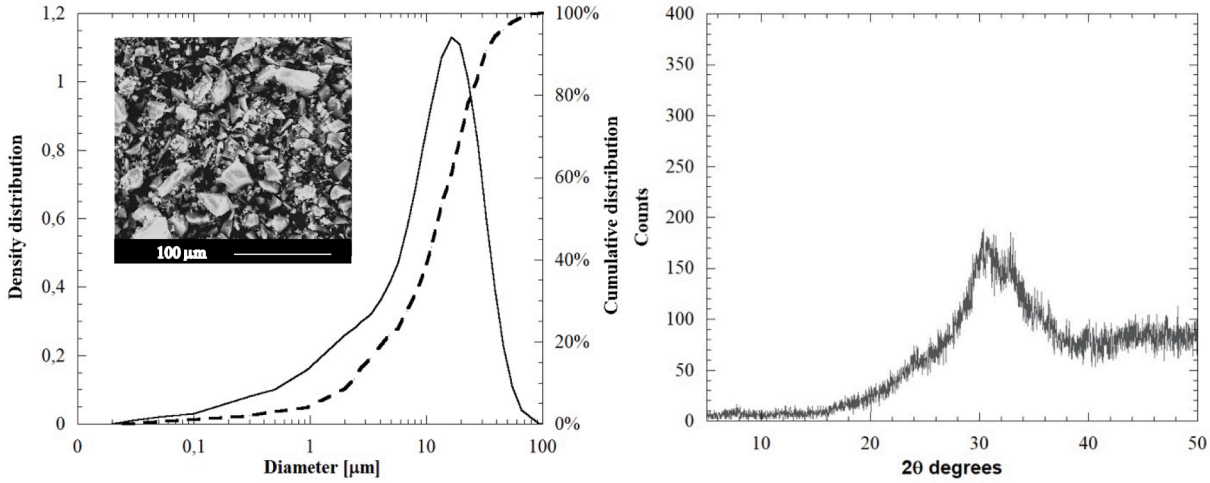

Fig. 1. Laser granulometry (on the left). SEM analyses of GGBFS (on the top left) and XRD pattern (on the right) of GGBFS.

Table 1
Chemical composition of GGBFS.

Component	CaO	Al_2O_3	SiO_2	SO_3	Fe_2O_3	TiO_2	K_2O	MgO
wt.%	45.56	10.35	32.93	1.58	0.23	2.25	0.72	6.38

Table 2
Composition of AAS pastes.

Composition [g]	Sp0	Sp1	Sp2	Sp3	Sp4	Sp5	Sp6
GGBFS	100	100	100	100	100	100	100
$Na_2SiO_3 \bullet 5\ H_2O$	–	1.26	2.52	5.04	10.08	15.12	20.16
KOH	–	0.54	1.08	2.16	4.32	6.48	8.64
Na_2CO_3	–	0.18	0.36	0.72	1.45	2.18	2.90
Water	30	30	30	30	30	30	30
Ms	–	0.48	0.48	0.48	0.48	0.48	0.48
Ac	–	0.0095	0.0190	0.0380	0.0750	0.1120	0.1500
w/s	0.30	0.30	0.30	0.31	0.32	0.32	0.33
a/p	–	0.014	0.027	0.054	0.109	0.163	0.218

2.4. Hardened state tests

Specimens 40 × 40 × 160 mm^3 and 10 × 10 × 10 mm^3 were produced (Table 3), cured for 24 h in steel mold covered by plastic films and stored in a climatic chamber at 20 °C and R.H. 60 %. Specific mass, compressive and flexural strength at 1, 7 and 28 days of pastes were also determined (EN 1015-11). Furthermore, dynamic modulus of elasticity was measured by means of Ultrasonic Digital Indicator Tester at 1, 7 and 28 days from casting (EN 12504-4). The tester gives the time value of the ultrasonic pulse through the specimens (in μs), then the velocity pulse value can be calculated by the Eq. (5):

$$v = \frac{l}{t} \tag{5}$$

with v: velocity of the ultrasonic pulse (m/s); l: length of specimen (m); and t: time of the sonic wave to go through the specimens (s). Knowing the velocity pulse, the dynamic modulus of elasticity (E_d, Eq. (6)) can be calculated by the following equation:

$$E_d = \frac{v^2\rho[(1+\gamma_d)(1-2\gamma_d)]}{(1-\gamma_d)} \tag{6}$$

with E_d: dynamic modulus of elasticity (GPa); v: velocity of the ultrasonic pulse (m/s); ρ: specific mass at hardened state (kg/m^3) and γ_d: Poisson's modulus. The Poisson's modulus, equal to 0.20, was estimated as the mean value between 0.15 and 0.25, as reported in literature for cementitious materials [40].

X-ray diffraction (XRD) and thermogravimetric analysis (TGA) were used to determine the mineralogical composition of the solid phase and water content. Prior to analysis, pastes were ground to a grain size < 63 μm.

The thermogravimetric analyses were carried out, in static air, using a Netzsch STA 409, at a heating rate of at 10 °C/min up to 820 °C and 10 mg of sample. Each sample was tested three times and the representative behavior was reported.

Table 3
Specimens manufactured for each paste.

Test	Ages	Specimen size	Number of specimens	Note
Flexural and compressive strength	1–7–28 days	Beam 40x40x160 mm^3	9	3 specimens for each age
Dynamic modulus of elasticity and specific mass	1–7–28 days	Beam 40x40x160 mm^3	9	3 specimens for each age
SEM/EDS	28 days	Cube 1 cm^3	2	–
TGA, DSC, FT-IR	28 days	Cube 1 cm^3 milled	3	–
XRD	1–2-7–28 days	Cube 1 cm^3 milled	8	2 specimens for each age

XRD data were collected using a Rigaku Miniflex diffractometer in a θ-2θ configuration using an incident beam monochromator employing the Cu Kα radiation (λ = 1.5418 Å) in a range of 5°-50° (2θ) with a step size of 0.02° and a step rate of 1°/min.

Analyses were performed at the scanning electron microscope (SEM), FEI model INSPECT, in order to investigate the microstructure of AAS pastes. Moreover, in order to evaluate the reacted slag, the protocol given by Luke and Glasser [41] and recently used by Kocaba [42], based on selective dissolution, was adopted.

By considering that the selective dissolution dissolves the hydration products, leaving only the unreacted slag grains as residue, the degree of hydration can be then calculated as (Eq. (7):

$$a_{SLAG}^{selectivedissolution} = \frac{m_{sample} - m_{residue}}{m_{sample}} \times 100 \quad (7)$$

Where:

m_{sample}: mass of the sample.

$m_{residue}$ = mass of undissolved residue from the sample.

The FT-IR transmittance spectra of the alkali activated samples were obtained using a Spectra FT/IR-4600 equipped with DLATGS IR Detector, a Ge/KBr beam splitter, and a high-intensity ceramic light source. Spectra were recorded between 450 cm^{-1} and 4000 cm^{-1}, with a resolution of 4 cm^{-1}.

3. Results and discussion

3.1. XRD analyses

Fig. 2 shows the X-ray diffraction data collected from AAS pastes with Ms = 0.48 and Ac = 0.075 up to 28 days of curing.

The major X-ray crystalline phase identified the aluminum containing C-S-H (C-A-S-H). An increased intensity of the C-S-H peaks was observed at longer curing ages, due to increase in the degree of crystallinity or by an increased formation of such phase as reported in [43]. Moreover, hydrotalcite (Ht) and of strätlingite (St) are also present in AAS pastes already after 2 days from casting. The observed assemblage of phases is in agreement with other articles related to GGBFS activated with sodium silicate [35,44,45]. The XRD patterns also show a contribution from non-crystalline fraction, as noted by the amorphous hump around 2θ = 25° − 35°, from the glassy unreacted slag [43]. In particular, after 1 day of curing, only the characteristic peak at 2θ = 29.7° of C-(A)-S-H was identified. Starting from two days of curing, it is possible to identify the peaks related to hydrotalcite, calcite and strätlingite, in good agreement with the ones expected from the models proposed by Ben Haha *et al.* [71] [46]. In particular, the thermodynamic models (Fig. 3) forecast, for the alkaline activation of GGBFS with a content of alumina and magnesium oxide equal to 10.35 % and 6.38 % respectively, the formation of high amount of calcium silicate hydrates accompanied by hydrotalcite and strätlingite.

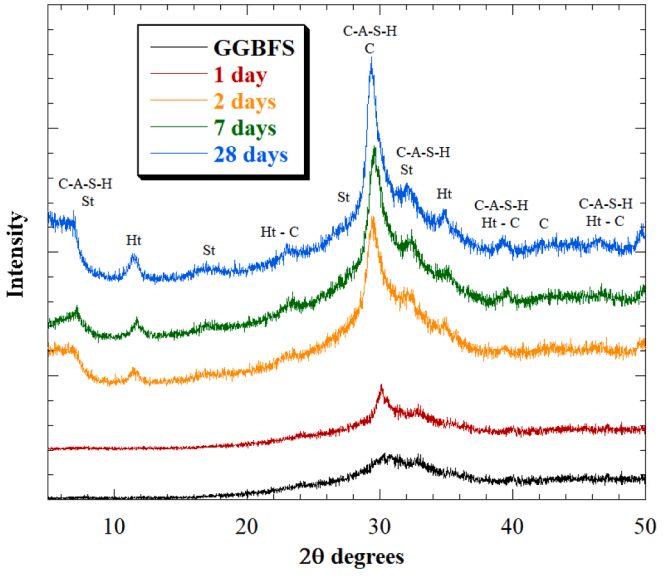

Fig. 2. XRD patterns of Sp4 sample at different ages of curing; Ht = Hydrotalcite (CSD n° 9009272(COD)); C = calcite (CSD n° 4502443(COD)); St = strätlingite (CSD n° 9005059(COD)); C-A-S-H = calcium aluminum silicate hydrate (PDF 00–034-0002).

No peaks related to zeolites were identified at early age of reaction (1–7 days) indicating that, in the selected proportion and amount of activators, the consumption of calcium ions by carbonate ions towards the formation of carbonates, did not lead to saturation of silicon and aluminum species with respect to aluminosilicate zeolite type products in the sodium-hydroxide-rich pore solution.

Fig. 4 illustrates X-ray diffractograms of AAS pastes with various alkali content (Ac), after 28 days of curing at 20 °C. All the samples show formation of C-(A)-S-H, in agreement with previous papers for similar systems [44,47,48]. The C-(A)-S-H peak intensity increased with higher alkali content within the system, consistent with the higher degree of reaction identified by thermogravimetric analysis and elasto-mechanical data discussed in the next paragraphs.

Furthermore, peaks of a hydrotalcite-type phase were also identified when Ac is greater than 0.0095 while strätlingite are present in pastes with Ac = 0.0750 ÷ 0.1500. This is in agreement with Song and Jennings [49], who have reported that hydrotalcite apparently forms when an high degree of slag hydration is reached. On the other hands, the mixing of GGBFS with water only determines the formation of small amounts of C-(A)-S-H as also reported by Park *et al.* [50]. Calcium carbonate in polymorphs of calcite and metastable vaterite was also identified. It is produced by the preferential early-age reaction between dissolved carbonate ions present in the pore solution and the calcium ions released by the partial dissolution of the slag [28]. Vaterite was identified in Sp0-Sp3 pastes. This metastable phase is stabilized, in these systems, by a sufficient high concentration of magnesium in the pore solution [51].

3.2. TGA measurements

The thermograms (TGA and DTA) of alkali activated slag pastes with various Ac at 28 days from casting are shown in Fig. 5. The mass loss between 30 °C and 120 °C is observed for all the samples, attributed to the release of evaporable water. In particular, the total mass loss up to 120 °C increases from 3 % for the pastes activated with Ac = 0.0095 to 9 % for the pastes with Ac greater than 0.1120. The exception is the paste Sp0 manufactured without activators, which is totally anhydrous.

The Non-Evaporable Water (NEW) provides a semiquantitative indicator for the reactivity of the slag as indicated by Escalante-Garcia *et al.* [45,52]. In particular, NEW was estimated by means of thermal analysis as (eq. (8):

$$NEW = 100 \bullet \frac{(weight_{120^\circ C} - weight_{820^\circ C})}{weight_{820^\circ C}} \quad (8)$$

Fig. 6 presents the results of NEW for AAS pastes at different alkali content (Ac). As reported by Escalante-Garcia *et al.* [45], the increase in concentration of activators (expressed as an increase in Ac) resulted in higher NEW values and strong activity at 28 days from casting. In particular, the bound water content obtained by measuring the weight loss between 120 °C and 180 °C using TGA is related with the dehydration of C-(A)-S-H [53] while the weight loss between 300 °C and 400 °C is assigned to the decomposition of hydrotalcite [54].

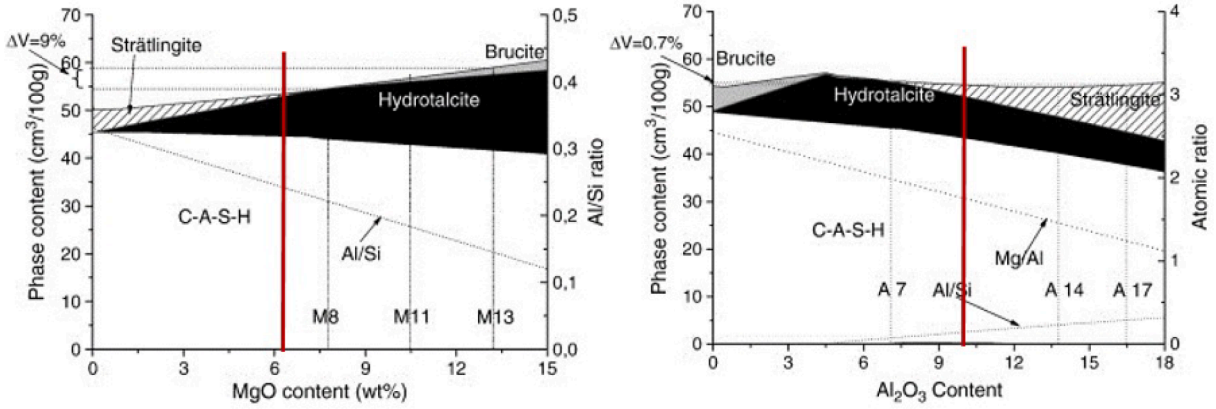

Fig. 3. Influence of MgO content (on the left) and alumina content (on the right) on the hydrates present in alkali activated slag.

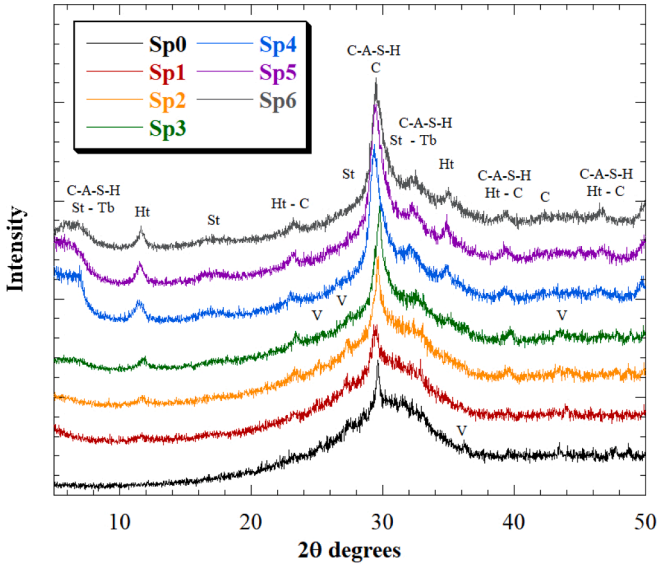

Fig. 4. XRD patterns of AAS pastes at 28 days from casting; Ht = Hydrotalcite (CSD n° 9009272(COD)); C = calcite (CSD n° 4502443(COD)); V = vaterite (CSD n° 9015898(COD)); St = strätlingite (CSD n° 9005059(COD)); C-A-S-H = calcium aluminium silicate hydrate (PDF 00–034-0002).

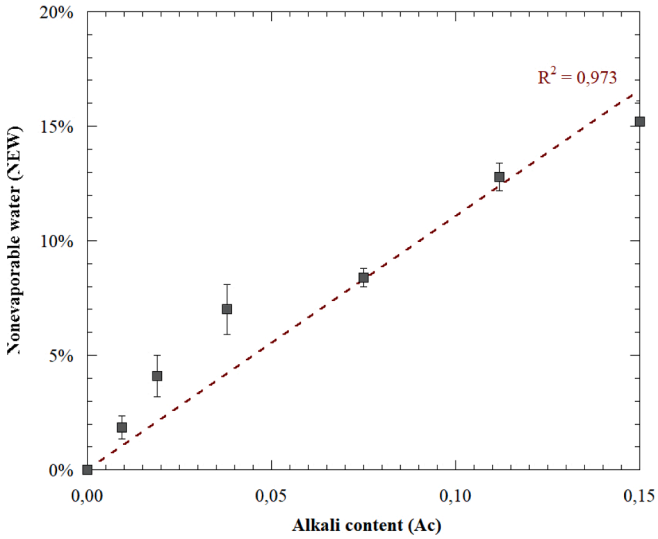

Fig. 6. Nonevaporable water (NEW) vs alkali content (Ac) at 28 days from casting.

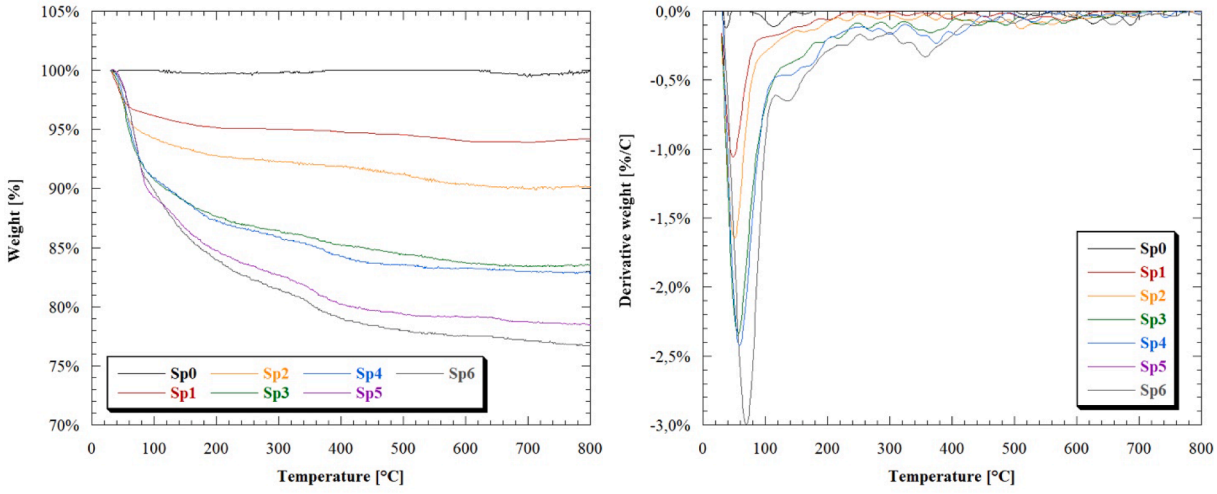

Fig. 5. Thermograms (cumulative on the left, derivative on the right) of AAS pastes cured for 28 days, with various alkali content (Ac).

3.3. SEM observations

The polished sections of the pastes were analyzed using SEM at an accelerating voltage of 20 kV. Microstructures are reported in Fig. 7.

The increasing of silicate and Na_2O content in mix design leads to a denser and more homogenous microstructure of pastes [43,55,56]. In samples Sp1, Sp2, Sp3 the microstructure is characterized by two main distinguishable phases: unreacted slag grains (USG) and activated gel products (outer products OP), with a limited formation of C-S-H gel confined around the unreacted slag particles. A significant alteration of the microstructure is observed between Sp3 and Sp4 samples, due to higher reaction of slag that furtherly increases in Sp5 and Sp6, due the greater content of activators. The formation of a reaction ring around the slag grains (inner product—IP) is also observable.

The results of the tests concerning the evaluation of reacted slag, carried out on Sp1, Sp5 and Sp6 pastes with three repetitions, are shown in Fig. 8. The amount of reacted slag increases with the increases of the activator's contents, with a remarkable step between Sp1 and Sp5, thus confirming the microstructural evidences.

The reliability of the selective dissolution was studied by analyzing the residues using X-ray diffraction (Fig. 9).

As it can be observed dissolution method succeeded in removing most of the hydration products, leading to residues that contain calcium carbonate as crystalline phase. Traces of C-A-S-H, and hydrotalcite are still detected in residues from the more reacted mixes.

3.4. FT-IR analyses

Infrared spectra of samples Sp1, Sp5 and Sp6 are reported in Fig. 10. The vibrational spectra of all samples can be divided into three groups of bands, related to the stretching and bending vibrations of water molecules and O–H groups, to CO_3^{2-} vibration and finally to the silicate tetrahedra vibrations. They can be analyzed individually because they

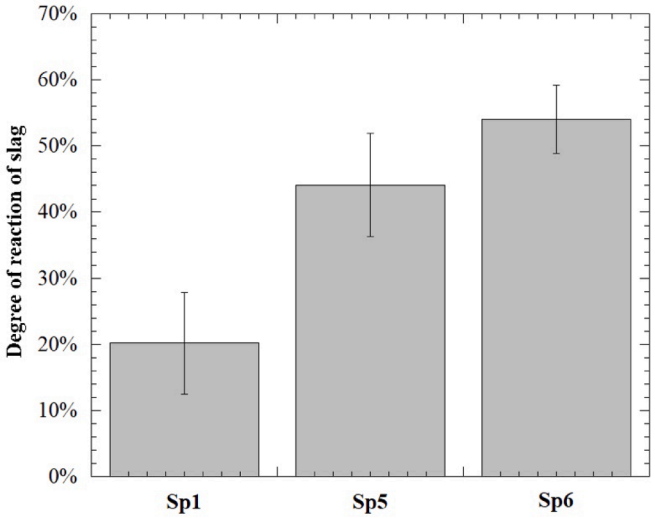

Fig. 8. Degree of slag reaction in Sp1, Sp5 and Sp6 according to Luke and Glasser protocol.

are not coupled [57,58].

The wide and poorly resolved region between 2900 and 3700 cm^{-1} can be attributed to hydrogen-bonded surface hydroxyl stretching vibrations of H_2O molecules. The broadening can be attributed to the wider range of the hydrogen bonding strengths. In particular, the band centered at 3600 cm^{-1} is attributed less strongly hydrogen-bonded interlayer water molecules. The broad peak centered near 3000 cm^{-1}, instead, relates to the O–H stretch of strongly polarized H-bonded water in the interlayer of the cementitious minerals and to O-H stretching of hydroxyl groups hydrogen-bonded to interlayer carbonate anions. This band shifts to lower frequencies from Sp1 to Sp6 samples due to the

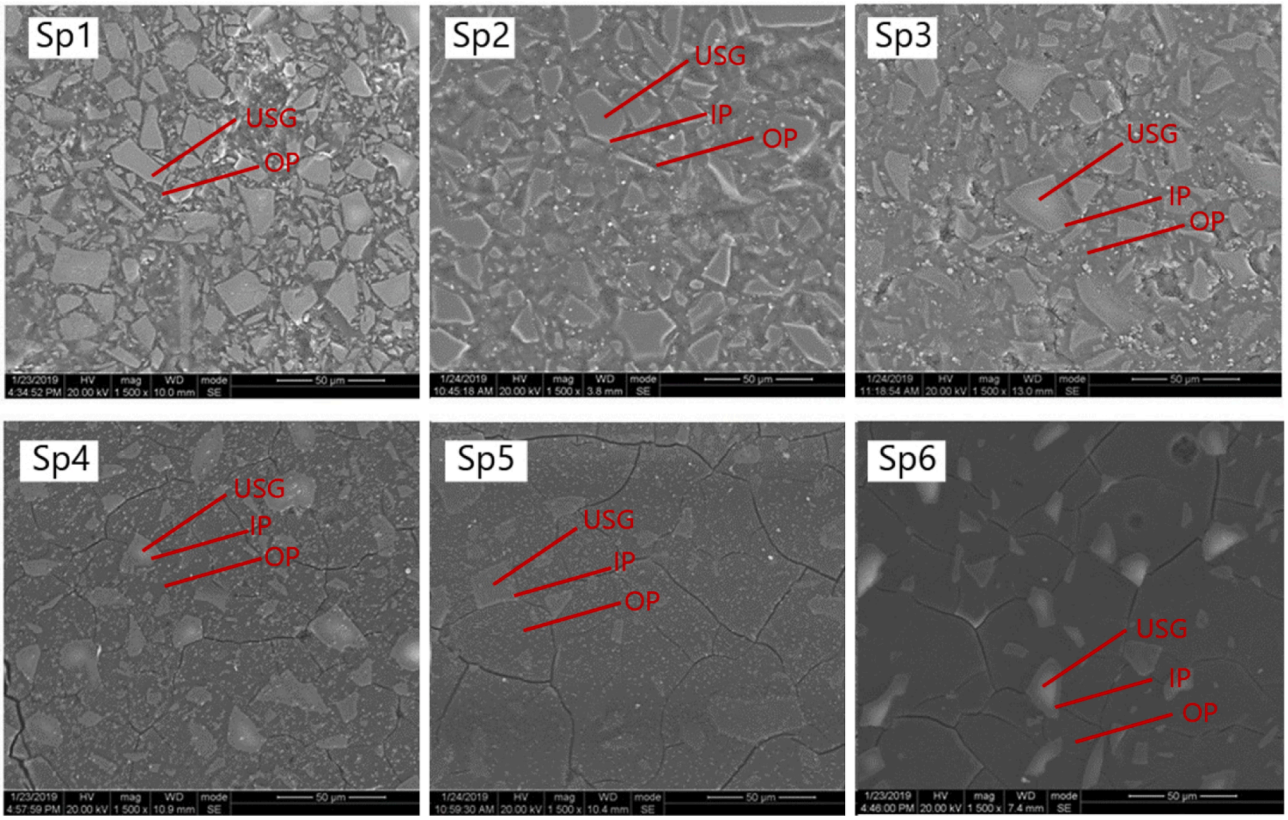

Fig. 7. SEM images at 1500x of Sp1-Sp6 pastes.

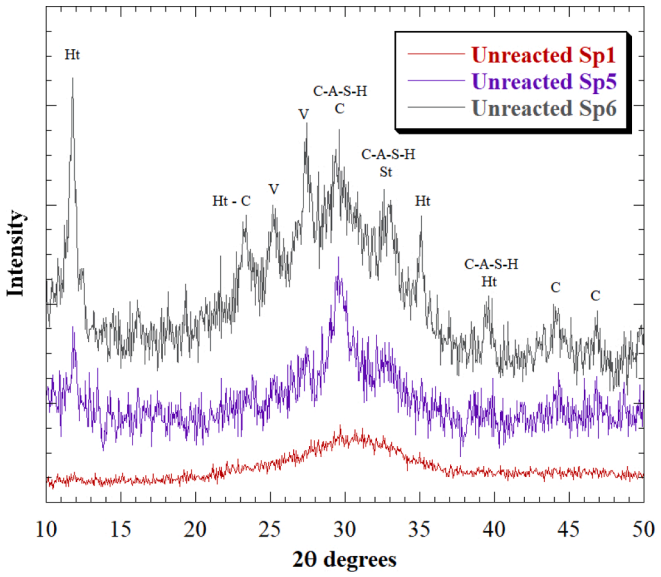

Fig. 9. XRD of the dissolution process residues of slag as is, Sp1, Sp5 and Sp6 Ht = Hydrotalcite (CSD n° 9009272(COD)); C = calcite (CSD n° 4502443 (COD)); V = vaterite (CSD n° 9015898(COD)); St = strätlingite (CSD n° 9005059(COD)); C-A-S-H = calcium aluminium silicate hydrate; (PDF 00–034-0002).

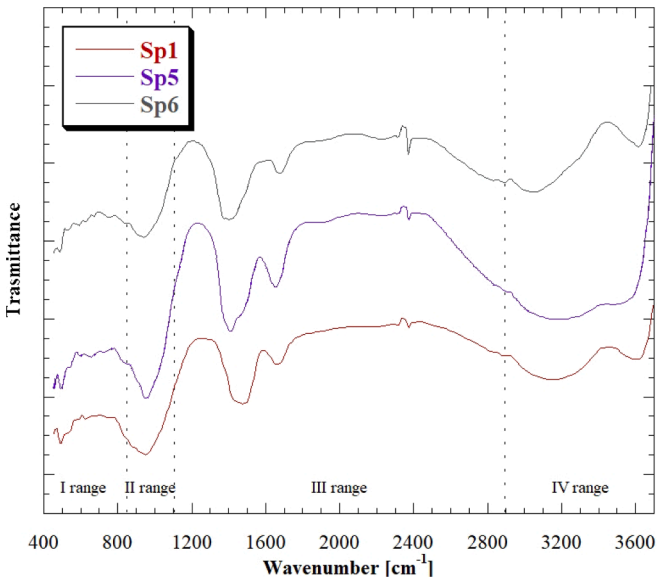

Fig. 10. Infrared spectra of Sp1, Sp5 and Sp6 samples.

increase in hydrogen bonding strength that can be attributed to the greater amount of activators used. Band at 1650 cm^{-1}, is related to O-H bending mode of molecular water and can be related to chemically combined water in the hydration products formed after activation [59]. The net small peak at 2900 cm^{-1} is due to the hydrogen bonding of H_2O and interlayer of SO_4^{2-} anions in hydrotalcite. Commonly accepted impurities of the sample inserted during preparation and handling of the KBr pellets are causing weak bands around 2800 cm^{-1} (C-H vibrations).

The principal infrared spectral features of silicates are localized as a complex group of bands in the range of 1100–850 cm^{-1}, and they can be attributed to the stretching modes of the SiQ^n(mAl) units. In particular n = 4, 3, 2, 1, and 0 are usually localized around 1200, 1100, 950, 900, and 850 cm^{-1}, respectively. All the examined samples show no sharp bands in the region that indicates a wide distribution of bonds stretching modes of the SiQ^n(mAl) units occurring in pastes. These findings indicate a poorly ordered structure and confirm XRD results. For all the samples, the characteristic set of bands is centered at around 960 cm^{-1}. It can be associated to the Si O asymmetric stretching vibrations due to the significant presence of Q^2 tetrahedra. Paste with low silicate and soda content (Sp1) shows a pronounced shoulder at the lower wavenumbers of the silicate region that can be associated to the presence Q^1 and Q^2 units. In pastes with higher activators content (Sp5 and Sp6 samples) the shoulder shifts to the higher wavenumbers due to the presence of more polymerized units such as Q^2 and Q^3 units. These changes in spectra indicate a variation in the structural characteristics of the pastes, as confirmed by XRD analyses and mechanical properties.

In Fig. 11 the decomposed spectra of Sp1, Sp5 and Sp6 in the region of CO_3^{2-} bands are showed.

The presence amorphous calcium carbonate (ACC) can be assessed by the splitting of U_3 band in ~ 1415 cm^{-1} and ~ 1466 cm^{-1} (ν_3) bands generating a clearly noticeable shoulder [60]. The interaction, upon intercalation, of CO_3^{2-} with OH groups found in the octahedral structure of the cationic layer of hydrotalcite, due to its strong electrostatic interactions in the symmetry-restricted interlayer space, produce the splitting of the band at 1415 cm^{-1} on either side of the wavenumber 1415 cm^{-1}, as a consequence of its lowered D3h symmetry. The band at ~ 1510 cm^{-1} belongs to an asymmetric stretching vibration of the C = O double bond τ(C = O) and represents the interaction of the CO_3^{2-} anion with OH groups found in the octahedral structure of the cationic layer of HT, whereas band at ~ 1360 cm^{-1} can be attributed to (C—O)—OH (interaction). Wavenumber (cm^{-1}) of the bands in the different samples are listed in Table 4.

As it can be noted in Fig. 11, shoulder becomes weaker with the increasing of the amount of activators used in the mixtures. The higher reaction of slag in Sp5-Sp6 systems promotes the formation of higher amount of magnesium-rich layered double hydroxides with a hydrotalcite type structure, as evidenced by X-ray analysis, that lowers the concentration of magnesium ions (Mg^{2+}) in the pore solution, therefore minimizing its effect in hindering calcite formation.

3.5. Fresh state properties

As it happens in the case of liquid activators, workability of the one-pot AAS is highly influenced by the alkali content at constant *Ms*. Fig. 12 shows that increasing the alkali content through the addition of growing amount of activators, the consistency of AAS pastes increases. In particular (Table 5), the non-activated or weakly alkali activated pastes exhibit a thixotropic consistency (about 150 mm spreading by flow table) while greater dosages of alkaline powders allow to obtain high flowable pastes (spread higher than 200 mm). This behavior is in accordance with [61] that explain the plasticizing and deflocculating effects of sodium silicate on alkali-activated slag-based mixtures with the increasing of the magnitude of repulsive double layer electric forces, causing the reduction in the yield stress at early ages.

None of the tested systems succeeded in extending the setting times. When lower amount of activators has been used, pH can't rise to values that favor slag dissolution and the loss of plasticity mainly arises from the extended induction period. When higher amounts of solid activators have been used, the early dissolution of calcium ions from slag grains has soon exceeded the amount that could react with carbonate ions (CO_3^{2-}), thus leading to calcium silicate hydrate formation [62–64], promoted by silicon ions provided by metasilicate dissolution. Its fast formation is responsible, in this case, of the measured short pot life (Fig. 13).

3.6. Hardened state properties

Fig. 14 shows how specific mass of AAS-pastes is affected by alkali content.

The increases from 2010 kg/m^3 to 2090 kg/m^3 in the specific mass of pastes at fresh state can be attributed to the increasing of the amount of

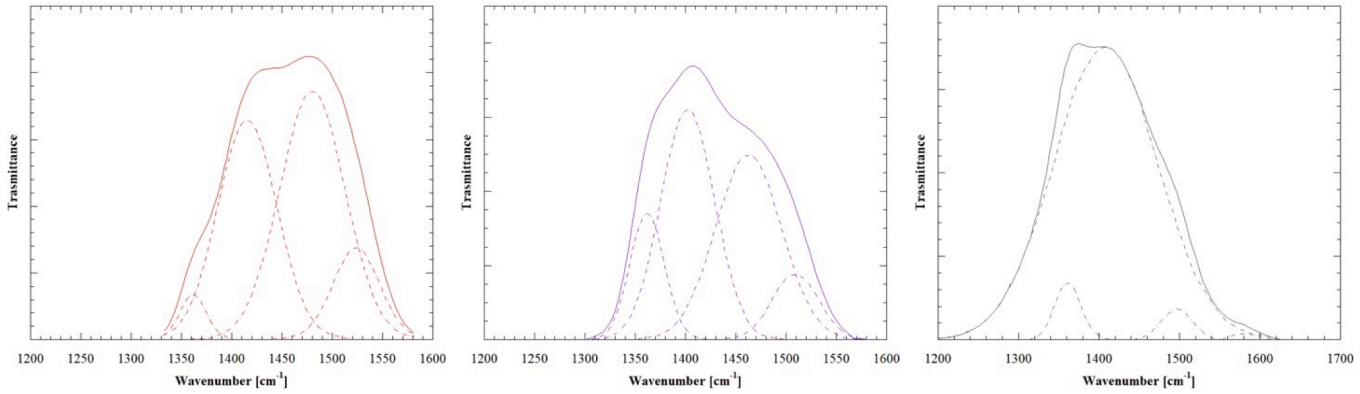

Fig. 11. Decomposed CO_3^{2-}bands of Sp1(left), Sp5 (center) and Sp6 (right) samples.

Table 4
FT-IR CO_3^{2-} decomposed bands.

Band cm^{-1} Sample	(C–O)–OH (interaction)	asymmetric υ_3 CO_3	asymmetric υ_3 CO_3	τ (C = O)
Sp1	1361	1415	1480	1523
Sp5	1361	1402	1462	1509
Sp6	1361	1408	1497	1579

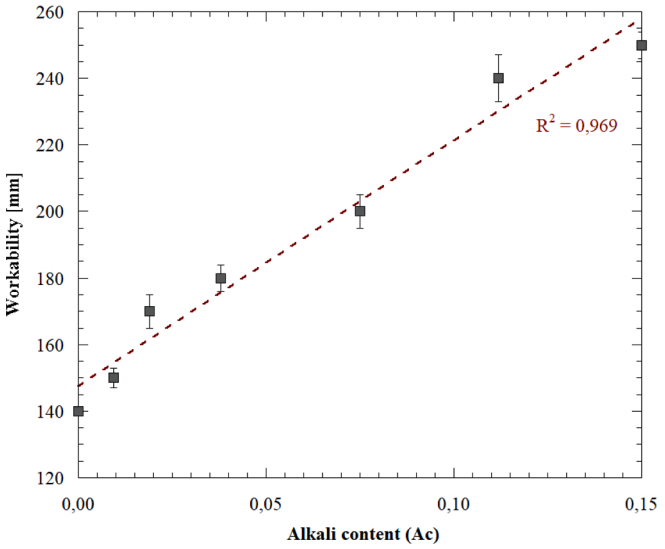

Fig. 12. Workability of AAS pastes by flow table vs alkali content (Ac).

the solid phase activators. A reduction in the difference between the specific mass at the fresh and hardened state with the increasing of the alkali content, is also observed. It can be, instead, attributed to the higher content of nonevaporable water (NEW) as a consequence of the higher degree of reaction of GGBFS, as confirmed by thermogravimetric analyses (Fig. 5) and the result by Luke and Glasser protocol (Fig. 8).

3.7. Elasto-mechanical properties

Compressive and flexural strength (Table 6) are strongly influenced by the alkali content. In particular, after 24 h, no-activated pastes were not enough hardened to measure mechanical properties while increasing the Ac allows to obtain mixtures with high 1-day strength, up to about 50 MPa. All the pastes show an increasing in the mechanical properties with time, in the investigated period, with compressive strength values close to 50–65 MPa at 7 days, achieving 28-day compressive strength up to 100 MPa. Also, the dynamic modulus of elasticity is strictly related with the dosage of the activators and to the developed mechanical properties.

Fig. 15 shows the effect of alkali content Ac on compressive strength of pastes at different ages. Mechanical properties at 1 day increase with the increasing of activators' content. Higher silicate and alkali content, at constant *Ms* cause higher Ca^{++} dissolution rate and promote its reaction with silicate ions to form C-A-S-H gel, whereas lower solid

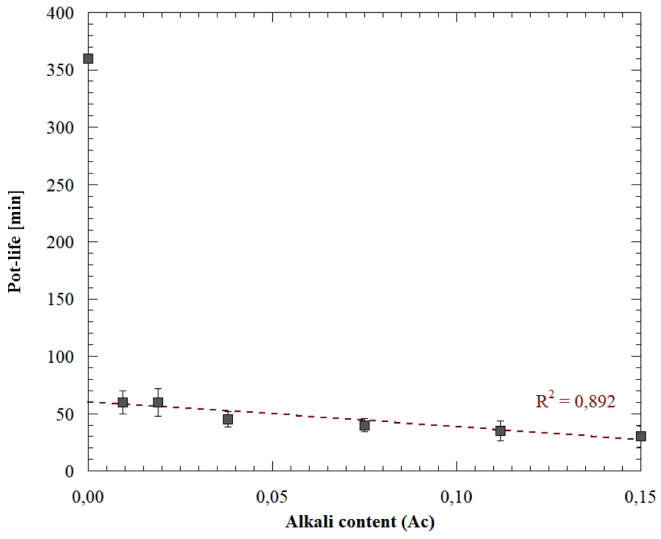

Fig. 13. Pot-life of AAS pastes vs alkali content (Ac). Sp0 was not taken into account for linear correlation.

Table 5
Fresh properties of AAS pastes.

		Sp0	Sp1	Sp2	Sp3	Sp4	Sp5	Sp6
Workability [mm]		140	150	170	180	200	240	250
Specific mass [kg/m^3]	Fresh state	2010	2015	2025	2040	2050	2060	2090
	Hardened state	1950	1970	1985	2010	2025	2045	2085

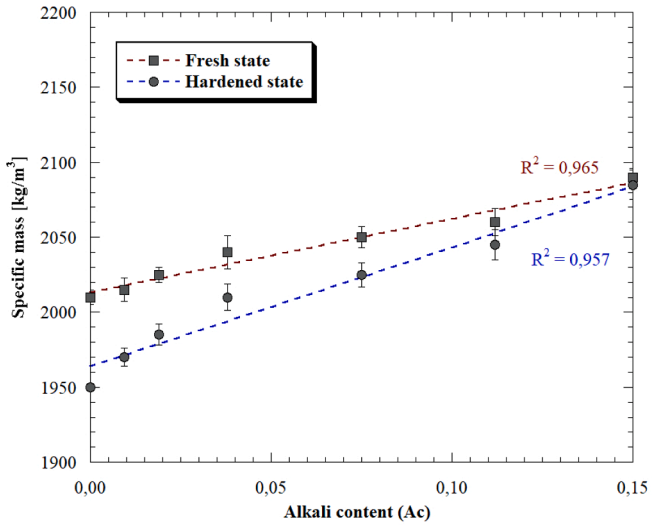

Fig. 14. Specific mass at fresh and hardened state of AAS pastes vs alkali content (Ac).

activators content increases the induction period thus determining a delay in developing the early mechanical properties. At longer curing period, an optimal alkali content can be identified. Lower solid activators content (Sp1), providing low pH, limit the extent of reacted slag, as confirmed by the measures of the reacted slag (Fig. 10). Up to Ac close to 0.05 (between Sp3 and Sp4), the increase in the amount of the used alkaline silicate solid activator determines a faster development of the mechanical properties and a higher strength final values. This behavior depends on the synergic effect of the different activators used during the production of AAS-pastes. Potassium hydroxide provides both hydroxide anion (OH^-) which is very important for the dissolution of the aluminosilicates in the first stage [65] and alkali cation (K^+) which is important for charge balance of the aluminosilicate network formed in the last stage [47]. As reported by Tang and Su-Fen [66], solubility of aluminosilicate increases with increasing OH^- concentration. Sodium silicate also provides good interparticle bonding and therefore mechanical strength of the material by synthetizing C-S-H gel as explained by Lecomte *et al.* [67]. Sodium carbonates promote the development of more cross-linked structured N-C-A-S-H gel and form precipitates along with carbonate salts [68,69] as confirmed by FT-IR analyses. Furtherly increase of Ac values, negatively affects the development of strength at longer curing time (Fig. 15), with decrements around 10–15 % after 28 days of curing. The behavior can be likely attributed to the formation of micro-cracks patterns produced by the higher shrinkage associated to the higher degree of slag reaction and from carbonation phenomena caused by the addition of excessive amounts of alkali that are not incorporated in stable products, as confirmed by SEM and FT-IR analyses. The results suggest that prolonged curing periods are necessary to assess reliable information about the evolution or degradation of the mechanical properties of AAS binders [64,70].

Finally, it can be observed a strong correlation between compressive strength and elastic modulus at different ages (Fig. 16) in accordance with the power law with exponent 0.3 proposed by EuroCode 2 (EN 1992–1-1) reported in Eq. (9). Known the compressive strength (CS), this relationship can be conveniently used to estimate the dynamic modulus of elasticity (E_d) of alkali activated pastes with different alkali content (for Sp0 the estimation is not reliable) by using a k equal to 12.5.

$$E_d = k \bullet \left(\frac{CS}{10}\right)^{0.3} \tag{9}$$

4. Conclusions and future trends

In this study, authors proposed a blend of solid activators, based on sodium metasilicate pentahydrate, potassium hydroxide and sodium carbonate, with the aim to furtherly widen the database of knowledge of one-part AAS binder. It was highlighted that the composition and the amount of alkaline activator influenced the workability, the kinetics of the reaction, the pot-life and the specific mass of pastes. High alkali content results in more flowable pastes characterized by a short pot-life and, at the hardened state, by a denser and more refined microstructure. Low alkali content reduced the degree of reaction, lead to the formation of amorphous calcium carbonate as well as metastable vaterite, without improving the pot-life as loss of plasticity occurred due to the extended induction period. High alkali contents negatively affect the mechanical

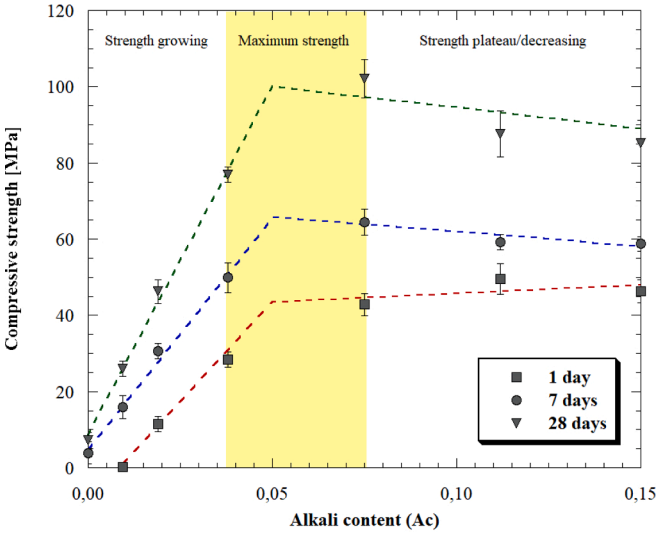

Fig. 15. Compressive strength of AAS pastes vs alkali content (Ac). Bimodal linear correlation with slope change at Ac close to 0,05.

Table 6
Elasto-mechanical properties of AAS pastes.

		Sp0	Sp1	Sp2	Sp3	Sp4	Sp5	Sp6
Flexural strength [MPa]	1 day	-	0.14	1.45	3.05	4.05	3.38	3.73
	7 days	0.45	1.15	2.18	4.19	5.21	4.88	4.91
	28 days	0.70	1.33	2.92	4.36	5.39	5.03	5.12
Compressive strength [MPa]	1 day	–	0.13	11.43	28.40	42.81	49.59	46.31
	7 days	3.94	15.90	30.59	49.88	64.44	59.28	58.72
	28 days	7.33	26.08	46.24	76.89	102.07	87.58	85.18
Elastic modulus [GPa]	1 day	–	–	13.33	17.95	20.75	20.75	21.09
	7 days	1.92	13.79	18.15	21.70	22.78	22.28	23.12
	28 days	6.20	17.04	21.31	25.41	26.14	25.06	25.30

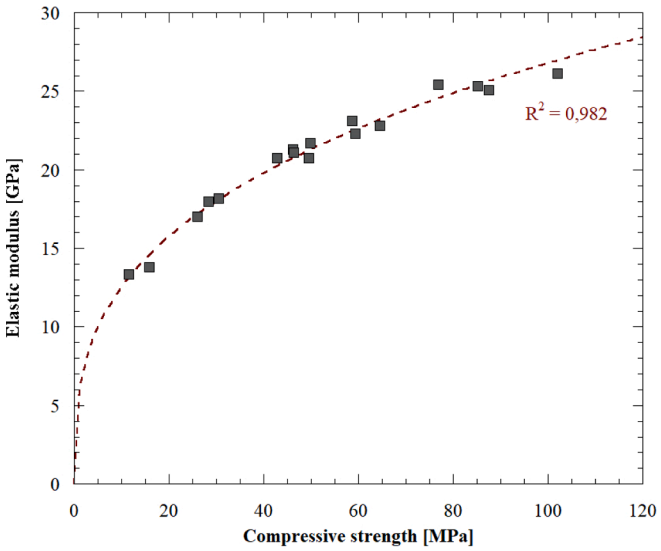

Fig. 16. Dynamic modulus of elasticity vs alkali content (Ac). The power correlation used was Ed = 12.5 · $(Rc/10)^{0,3}$ in accordance with EuroCode 2.

properties of pastes at later ages due to the formation of micro-cracks. Finally, it was determined that the optimal alkali content, balancing high flowability, favorable setting times, and excellent strength, lies in proximity to 0.075.

In forthcoming research endeavors, the variation of the molar silica modulus (Ms) and of the relative mass activators ratio, will be investigated with the objective to gain a comprehensive understanding of how to effectively tailor the properties of one-part alkali-activated materials.

CRediT authorship contribution statement

D. Coffetti: Writing – review & editing, Writing – original draft, Visualization, Methodology, Investigation, Conceptualization. **S. Candamano:** Writing – review & editing, Writing – original draft, Methodology, Investigation, Conceptualization. **F. Crea:** Writing – review & editing, Validation. **L. Coppola:** Writing – review & editing, Validation, Supervision, Resources, Conceptualization.

Declaration of Competing Interest

The authors declare that they have no known competing financial interests or personal relationships that could have appeared to influence the work reported in this paper.

Data availability

Data will be made available on request.

Acknowledgments

Authors would also to thank Giovanna Rotella for providing help during samples' polishing.

Appendix A. Supplementary data

Supplementary data to this article can be found online at https://doi.org/10.1016/j.conbuildmat.2023.133868.

References

[1] D. Coffetti, E. Crotti, G. Gazzaniga, M. Carrara, T. Pastore, L. Coppola, Pathways towards sustainable concrete, Cem. Concr. Res. 154 (2022), 106718, https://doi.org/10.1016/j.cemconres.2022.106718.

[2] A. Gruskovnjak, B. Lothenbach, F. Winnefeld, B. Münch, R. Figi, S.-C. Ko, M. Adler, U. Mäder, Quantification of hydration phases in supersulfated cements: review and new approaches, Adv. Cem. Res. 23 (2011) 265–275, https://doi.org/10.1680/adcr.2011.23.6.265.

[3] A. Telesca, M. Marroccoli, D. Coffetti, L. Coppola, S. Candamano, Tartaric acid effects on hydration development and physico-mechanical properties of blended calcium sulphoaluminate cements, Cem. Concr. Compos. 124 (2021), 104275, https://doi.org/10.1016/j.cemconcomp.2021.104275.

[4] G. Li, J. Zhang, Z. Song, C. Shi, A. Zhang, Improvement of workability and early strength of calcium sulphoaluminate cement at various temperature by chemical admixtures, Constr. Build. Mater. 160 (2018) 427–439, https://doi.org/10.1016/j.conbuildmat.2017.11.076.

[5] G. Ke, J. Zhang, Y. Liu, Shrinkage characteristics of calcium sulphoaluminate cement concrete, Constr. Build. Mater. 337 (2022), 127627, https://doi.org/10.1016/j.conbuildmat.2022.127627.

[6] T. Luukkonen, Z. Abdollahnejad, J. Yliniemi, P. Kinnunen, M. Illikainen, One-part alkali-activated materials: A review, Cem. Concr. Res. 103 (2018) 21–34, https://doi.org/10.1016/j.cemconres.2017.10.001.

[7] J.L. Provis, Alkali-activated materials, Cem. Concr. Res. 114 (2018) 40–48, https://doi.org/10.1016/j.cemconres.2017.02.009.

[8] L. Tefa, M. Bassani, B. Coppola, P. Palmero, Strength development and environmental assessment of alkali-activated construction and demolition waste fines as stabilizer for recycled road materials, Constr. Build. Mater. 289 (2021), 123017, https://doi.org/10.1016/j.conbuildmat.2021.123017.

[9] S. Candamano, P. De Luca, P. Frontera, F. Crea, Production of Geopolymeric Mortars Containing Forest Biomass Ash as Partial Replacement of Metakaolin, Environments 4 (2017) 74, https://doi.org/10.3390/environments4040074.

[10] C. Lamuta, S. Candamano, F. Crea, L. Pagnotta, Direct piezoelectric effect in geopolymeric mortars, Mater. Des. 107 (2016) 57–64, https://doi.org/10.1016/j.matdes.2016.05.108.

[11] S.A. Bernal, J.L. Provis, Durability of Alkali-Activated Materials: Progress and Perspectives, J. Am. Ceram. Soc. 97 (2014) 997–1008, https://doi.org/10.1111/jace.12831.

[12] M. Elzeadani, D.V. Bompa, A.Y. Elghazouli, One part alkali activated materials: A state-of-the-art review, J. Build. Eng. 57 (2022), 104871, https://doi.org/10.1016/j.jobe.2022.104871.

[13] B. Zhang, H. Zhu, Y. Cheng, G. Fahim, K. Wei, Shrinkage mechanisms and shrinkage-mitigating strategies of alkali-activated slag composites : A critical review, Constr. Build. Mater. 318 (2022), 125993, https://doi.org/10.1016/j.conbuildmat.2021.125993.

[14] R. Cai, H. Ye, Clinkerless ultra-high strength concrete based on alkali-activated slag at high temperatures, Cem. Concr. Res. 145 (2021), 106465, https://doi.org/10.1016/j.cemconres.2021.106465.

[15] M. Shariati, A. Shariati, N.T. Trung, P. Shoaei, F. Ameri, N. Bahrami, S. N. Zamanabadi, Alkali-activated slag (AAS) paste: Correlation between durability and microstructural characteristics, Constr. Build. Mater. 267 (2021), 120886, https://doi.org/10.1016/J.CONBUILDMAT.2020.120886.

[16] D. Jiang, C. Shi, Z. Zhang, Recent progress in understanding setting and hardening of alkali-activated slag (AAS) materials, Cem. Concr. Compos. 134 (2022), 104795, https://doi.org/10.1016/j.cemconcomp.2022.104795.

[17] Y. Zhang, Y. Fang, Y. Shen, Z. Yang, K. Wu, Chloride penetration and binding behavior in unsaturated alkali-activated slag mortars, Cem. Concr. Compos. 140 (2023), 105098, https://doi.org/10.1016/j.cemconcomp.2023.105098.

[18] C. Liu, X. Liang, Y. Chen, Z. Li, G. Ye, Degradation of alkali-activated slag subject to water immersion, Cem. Concr. Compos. 142 (2022), https://doi.org/10.1016/j.cemconcomp.2023.105157.

[19] W. Zhang, M. Xue, H. Lin, X. Duan, Y. Jin, F. Su, Effect of polyether shrinkage reducing admixture on the drying shrinkage properties of alkali-activated slag, Cem. Concr. Compos. 136 (2023), 104865, https://doi.org/10.1016/j.cemconcomp.2022.104865.

[20] Z. Abdollahnejad, M. Mastali, T. Luukkonen, P. Kinnunen, M. Illikainen, Fiber-reinforced one-part alkali-activated slag/ceramic binders, Ceram. Int. 44 (2018) 8963–8976, https://doi.org/10.1016/j.ceramint.2018.02.097.

[21] P. Perumal, H. Nguyen, V. Carvelli, P. Kinnunen, M. Illikainen, High strength fiber reinforced one-part alkali activated slag composites from industrial side streams, Constr. Build. Mater. 319 (2022), 126124, https://doi.org/10.1016/j.conbuildmat.2021.126124.

[22] S. Zhang, Y. He, H. Zhang, J. Chen, L. Liu, Effect of fine sand powder on the rheological properties of one-part alkali-activated slag semi-flexible pavement grouting materials, Constr. Build. Mater. 333 (2022), 127328, https://doi.org/10.1016/j.conbuildmat.2022.127328.

[23] S. Candamano, F. Crea, A. Iorfida, Mechanical characterization of basalt fabric-reinforced alkali-activated matrix composite: a preliminary investigation, Appl. Sci. 10 (2020), https://doi.org/10.3390/app10082865.

[24] D. Coffetti, E. Crotti, L. Coppola, Long-term properties of self-cleaning alkali-activated slag-based mortars with titanium dioxide nanoparticles, Constr. Build. Mater. 392 (2023), 131976, https://doi.org/10.1016/j.conbuildmat.2023.131976.

[25] D. Ravikumar, N. Neithalath, Effects of activator characteristics on the reaction product formation in slag binders activated using alkali silicate powder and NaOH, Cem. Concr. Compos. 34 (2012) 809–818, https://doi.org/10.1016/j.cemconcomp.2012.03.006.

[26] J. Provis, J. van Deventer, Alkali Activated Materials State-of-the-Art Report, in: RILEM TC 224-AAM, Springer, London, UK, 2014.

[27] S. Bernal, R. San Nicolas, J. Provis, J.s.j. van Deventer, Alkali-activated slag cements produced with a blended sodium carbonate / sodium silicate activator, Adv. Cem. Res. 28 (2015) 1–12.

[28] S.A. Bernal, J.L. Provis, R.J. Myers, R. San Nicolas, J.s.j. van Deventer, Role of carbonates in the chemical evolution of sodium carbonate-activated slag binders, Mater. Struct. Constr. 48 (2014) 517–529, https://doi.org/10.1617/s11527-014-0412-6.
[29] P. Duxson, J.L. Provis, G.C. Lukey, J.S.J. Van Deventer, F. Separovic, Z.H. Gan, 39K NMR of free potassium in geopolymers, Ind. Eng. Chem. Res. 45 (2006) 9208–9210, https://doi.org/10.1021/ie060838g.
[30] E. Najafi Kani, A. Allahverdi, J.L. Provis, Efflorescence control in geopolymer binders based on natural pozzolan, J. Therm. Anal. Calorim. 34 (2012) 25–33.
[31] A. Fernandez-Jimenez, F. Puertas, Effect of activator mix on the hydration and strength behaviour of alkali-activated slag cements, Adv. Cem. Res. 15 (2003) 129–136.
[32] P.O. Awoyera, A. Adesina, A. Sivakrishna, R. Gobinath, K.R. Kumar, A. Srinivas, Alkali activated binders: Challenges and opportunities, Mater. Today:. Proc. 27 (2020) 40–43, https://doi.org/10.1016/j.matpr.2019.08.199.
[33] S. Aydin, B. Baradan, Effect of activator type and content on properties of alkali-activated slag mortars, Compos. B Eng. 57 (2014) 166–172, https://doi.org/10.1016/j.compositesb.2013.10.001.
[34] B. Walkley, X. Ke, J.L. Provis, S.A. Bernal, Activator Anion Influences the Nanostructure of Alkali-Activated Slag Cements, J. Phys. Chem. C 125 (2021) 20727–20739, https://doi.org/10.1021/acs.jpcc.1c07328.
[35] S.-D. Wang, K.L. Scrivener, Hydration products of alkali activated slag cement, Cem. Concr. Res. 25 (1995) 561–571.
[36] S.-D. Wang, K.L. Scrivener, P.L. Pratt, Factors affecting the strength of alkali-activated slag, Cem. Concr. Res. 24 (1994) 1033–1043, https://doi.org/10.1016/0008-8846(94)90026-4.
[37] L. Coppola, D. Coffetti, E. Crotti, A. Marini, C. Passoni, T. Pastore, Lightweight cement-free alkali-activated slag plaster for the structural retrofit and energy upgrading of poor quality masonry walls, Cem. Concr. Compos. 104 (2019), https://doi.org/10.1016/j.cemconcomp.2019.103341.
[38] Y. Li, Y. Sun, Preliminary study on combined-alkali-slag paste materials, Cem. Concr. Res. 30 (2000) 963–966, https://doi.org/10.1016/S0008-8846(00)00269-6.
[39] R. Bayuaji, A.K. Yasin, T.E. Susanto, M.S. Darmawan, S. Darmawan, A review in geopolymer binder with dry mixing method (geopolymer cement), AIP Conf. Proc. 1887 (2017) 20042, https://doi.org/10.1063/1.5003513.
[40] A.M. Neville, Properties of concrete, Longman London, 1995.
[41] K. Luke, F.P. Glasser, Selective dissolution of hydrated blast furnace slag cements, Cem. Concr. Res. 17 (1987) 273–282, https://doi.org/10.1016/0008-8846(87)90110-4.
[42] V. Kocaba, E. Gallucci, K.L. Scrivener, Methods for determination of degree of reaction of slag in blended cement pastes, Cem. Concr. Res. 42 (2012) 511–525, https://doi.org/10.1016/j.cemconres.2011.11.010.
[43] O. Burciaga-Díaz, J.I. Escalante-García, Structure, mechanisms of reaction, and strength of an alkali-activated blast-furnace slag, J. Am. Ceram. Soc. 96 (2013) 3939–3948, https://doi.org/10.1111/jace.12620.
[44] Y.J. Zhang, Y.L. Zhao, H.H. Li, D.L. Xu, Structure characterization of hydration products generated by alkaline activation of granulated blast furnace slag, J. Mater. Sci. 43 (2008) 7141–7147, https://doi.org/10.1007/s10853-008-3028-9.
[45] J.I. Escalante-García, A.F. Fuentes, A. Gorokhovsky, P.E. Fraire-Luna, G. Mendoza-Suarez, Hydration products and reactivity of blast-furnace slag activated by various alkalis, J. Am. Ceram. Soc. 86 (2003) 2148–2153, https://doi.org/10.1111/j.1151-2916.2003.tb03623.x.
[46] M. Ben Haha, B. Lothenbach, G. Le Saout, F. Winnefeld, Influence of slag chemistry on the hydration of alkali-activated blast-furnace slag - Part II: Effect of Al2O3, Cem. Concr. Res. 42 (2012) 74–83.
[47] A. Allahverdi, E. Najafi Kani, S. Esmaeilpoor, Effects of Silica Modulus and Alkali Concentration on Activation of Blast-Furnace Slag, Iran. J. Mater. Sci. Eng. 5 (2008) 32–35. http://ijmse.iust.ac.ir/browse.php?a_code=A-10-3-26&slc_lang=en&sid=1.
[48] L. Coppola, D. Coffetti, E. Crotti, S. Candamano, F. Crea, G. Gazzaniga, T. Pastore, The combined use of admixtures for shrinkage reduction in one-part alkali activated slag-based mortars and pastes, Constr. Build. Mater. 248 (2020), https://doi.org/10.1016/j.conbuildmat.2020.118682.
[49] S. Song, H.M. Jennings, Pore solution chemistry of alkali-activated ground granulated blast-furnace slag, Cem. Concr. Res. 29 (1999) 159–170, https://doi.org/10.1016/S0008-8846(98)00212-9.
[50] H. Park, Y. Jeong, J.H. Jeong, J.E. Oh, Strength development and hydration behavior of self-activation of commercial ground granulated blast-furnace slag mixed with purified water, Materials (basel). 9 (2016), https://doi.org/10.3390/ma9030185.
[51] E. Loste, R.M. Wilson, R. Seshadri, F.C. Meldrum, The role of magnesium in stabilising amorphous calcium carbonate and controlling calcite morphologies, J. Cryst. Growth 254 (2003) 206–218, https://doi.org/10.1016/S0022-0248(03)01153-9.
[52] J.I. Escalante, L.Y. Gómez, K.K. Johal, G. Mendoza, H. Mancha, J. Méndez, Reactivity of blast-furnace slag in Portland cement blends hydrated under different conditions, Cem. Concr. Res. 31 (2001) 1403–1409, https://doi.org/10.1016/S0008-8846(01)00587-7.
[53] E. Tajuelo Rodriguez, K. Garbev, D. Merz, L. Black, I.G. Richardson, Thermal stability of C-S-H phases and applicability of Richardson and Groves' and Richardson C-(A)-S-H(I) models to synthetic C-S-H, Cem. Concr. Res. 93 (2017) 45–56, https://doi.org/10.1016/j.cemconres.2016.12.005.
[54] M. Bellotto, B. Rebours, O. Clause, J. Lynch, D. Bazin, E. Elkaïm, Hydrotalcite decomposition mechanism: A clue to the structure and reactivity of spinel-like mixed oxides, J. Phys. Chem. 100 (1996) 8535–8542, https://doi.org/10.1021/jp960040i.
[55] R.R. Lloyd, J.L. Provis, J.S.J. Van Deventer, Microscopy and microanalysis of inorganic polymer cements. 2: The gel binder, J. Mater. Sci. 44 (2009) 620–631, https://doi.org/10.1007/s10853-008-3078-z.
[56] R.J. Myers, S.A. Bernal, R. San Nicolas, J.L. Provis, Generalized structural description of calcium-sodium aluminosilicate hydrate gels: The cross-linked substituted tobermorite model, Langmuir 29 (2013) 5294–5306, https://doi.org/10.1021/la4000473.
[57] I. García Lodeiro, D.E. Macphee, A. Palomo, A. Fernández-Jiménez, Effect of alkalis on fresh C-S-H gels. FTIR analysis, Cem. Concr. Res. 39 (2009) 147–153, https://doi.org/10.1016/j.cemconres.2009.01.003.
[58] I. García-Lodeiro, A. Fernández-Jiménez, M.T. Blanco, A. Palomo, FTIR study of the sol-gel synthesis of cementitious gels: C-S-H and N-A-S-H, J. Sol-Gel Sci. Technol. 45 (2008) 63–72, https://doi.org/10.1007/s10971-007-1643-6.
[59] S.A. Bernal, R.M. de Gutierrez, J.L. Provis, V. Rose, Effect of silicate modulus and metakaolin incorporation on the carbonation of alkali silicate-activated slags, Cem. Concr. Res. 40 (2010) 898–907, https://doi.org/10.1016/j.cemconres.2010.02.003.
[60] J.D. Rodriguez-Blanco, S. Shaw, L.G. Benning, The kinetics and mechanisms of amorphous calcium carbonate (ACC) crystallization to calcite, via vaterite, Nanoscale 3 (2011) 265–271, https://doi.org/10.1039/c0nr00589d.
[61] A. Kashani, J.L. Provis, G.G. Qiao, J.S.J. van Deventer, The interrelationship between surface chemistry and rheology in alkali activated slag paste, Constr. Build. Mater. 65 (2014) 583–591, https://doi.org/10.1016/J.CONBUILDMAT.2014.04.127.
[62] Z. Huanhai, W. Xuequan, X. Zhongzi, T. Mingshu, Kinetic study on hydration of alkali-activated slag, Cem. Concr. Res. 23 (1993) 1253–1258, https://doi.org/10.1016/0008-8846(93)90062-E.
[63] J.J. Chang, A study on the setting characteristics of sodium silicate-activated slag pastes, Cem. Concr. Res. 33 (2003) 1005–1011, https://doi.org/10.1016/S0008-8846(02)01096-7.
[64] V. Živica, Effects of type and dosage of alkaline activator and temperature on the properties of alkali-activated slag mixtures, Constr. Build. Mater. 21 (2007) 1463–1469, https://doi.org/10.1016/j.conbuildmat.2006.07.002.
[65] F. Pacheco-Torgal, J. Labrincha, C. Leonelli, A. Palomo, P. Chindaprasirt, Handbook of alkali-activated cements, mortars and concretes, 2014.
[66] M.S. Tang, H. Su-Fen, Effect of Ca(OH)2 on alkali-silica reaction. Proc. 8th Int. Congr. Cem, Chem, 1980.
[67] I. Lecomte, C. Henrist, M. Liégeois, F. Maseri, A. Rulmont, R. Cloots, (Micro)-structural comparison between geopolymers, alkali-activated slag cement and Portland cement, J. Eur. Ceram. Soc. 26 (2006) 3789–3797, https://doi.org/10.1016/j.jeurceramsoc.2005.12.021.
[68] X. Hua, J.L. Provis, J.S.J. Van Deventer, P.V. Krivenko, Characterization of Aged Slag Concretes, ACI Mater. J. 105 (2008) 131–139. https://doi.org/10.14359/19753.
[69] A. Fernández-Jiménez, F. Puertas, I. Sobrados, J. Sanz, Structure of calcium silicate hydrates formed in alkaline-activated slag: influence of the type of alkaline activator, J. Am. Ceram. Soc. 86 (2003) 1389–1394.
[70] S.A. Bernal, J.L. Provis, V. Rose, R. Mejía De Gutierrez, Evolution of binder structure in sodium silicate-activated slag-metakaolin blends, Cem. Concr. Compos. 33 (2011) 46–54, https://doi.org/10.1016/j.cemconcomp.2010.09.004.
[71] M. Ben Haha, B. Lothenbach, G. Le Saout, F. Winnefeld, Influence of slag chemistry on the hydration of alkali-activated blast-furnace slag - Part I: Effect of MgO, Cem. Concr. Res. 41 (9) (2011) 955–963, https://doi.org/10.1016/j.cemconres.2011.05.002.